Photocurable Carbonaceous Composites with Tunable Piezoresistive Response

Advanced Composites and Hybrid Materials (2026) 9:251
https://doi.org/10.1007/s42114-026-01770-2

RESEARCH

Photocurable Carbonaceous Composites with Tunable Piezoresistive Response

Cristian Mendes-Felipe[1,2] · Luis Rubio-Peña[3] · Pedro Costa[4] · Viktor Petrenko[1,5] · Leide Passos Cavalcanti[6] · Mohamed Zbiri[7] · Maksym Golub[8] · Jörg Pieper[8] · Marco Sangermano[2] · Senentxu Lanceros-Mendez[1,4,5]

Received: 10 December 2025 / Revised: 22 March 2026 / Accepted: 27 March 2026

Abstract
Photocurable polymer composites with tailored electrical and mechanical properties is of growing interest for advanced manufacturing and (multi)functional applications. This study investigates how two carbonaceous fillers, carbon nanotubes (CNT) and reduced graphene oxide (rGO), affect the photopolymerization, nanoscale structure, and macroscopic properties of two photocurable resins with distinct mechanical nature: an elastic polyurethane acrylate (SPOT-E) and a rigid bio-based acrylated epoxidized soybean oil (AESO). Photorheology reveals that CNT strongly inhibit curing above 0.6 wt.% due to optical shielding, while rGO enables complete curing up to 5 wt.%. Dispersion analysis indicates homogeneous distributions for both fillers, whereas mechanical analysis exhibits network deterioration at high filler contents. Quasi-elastic neutron scattering shows that fillers incorporation significantly restricted SPOT-E dynamics but enhanced AESO mobility, the effect depending on filler type and loading filler contents. These multiscale effects translate into electrical conductivities of 0.014 S/m (SPOT-E/CNT) and $7.5 \cdot 10^{-5}$ S/m (AESO/rGO). Finally, piezoresistive assessment revealed maximum gauge factors of ~ 0.9 for SPOT-E/CNT and ~ 50 for AESO/rGO systems and stability over 700 cycles. These results provide essential insights into the interplay between filler morphology, photopolymerization, and multifunctional performance in UV-curable composites, enabling the rational design of materials with predefined properties for additive manufacturing and electronics applications.

Keywords Photocurable composites · Carbon nanotubes · Reduced graphene oxide · Neutron scattering · Electrical conductivity · Piezoresistive behavior

1 Introduction

Photocurable polymer composites are versatile materials for advanced manufacturing, offering rapid curing, energy efficiency, and compatibility with digital fabrication additive manufacturing technologies [1, 2]. These systems enable spatially controlled polymerization under light exposure, making them highly attractive for structural and functional applications, including flexible electronics, sensing, and stimuli responsive components [3]. Designing photocurable composites that simultaneously achieve excellent curing performance, tailored mechanical behavior, and

✉ Cristian Mendes-Felipe
cristian.mendes@bcmaterials.net

✉ Senentxu Lanceros-Mendez
senentxu.lanceros@bcmaterials.net

1 BCMaterials, Basque Center for Materials, Applications and Nanostructures, UPV/EHU Science Park, 48940 Leioa, Spain

2 Department of Applied Science and Technology (DISAT), Politecnico Di Torino, 10129 Turin, Italy

3 Engineering School, University of Cadiz, Avda. de La Universidad de Cádiz, 10, 11519 Puerto Real, Spain

4 Physics Centre of Minho and Porto Universities (CF-UM-UP) University of Minho, LaPMET – Laboratory of Physics for Materials and Emergent Technologies University of Minho, 4710-057 Guimarães, Portugal

5 Basque Foundation for Science, IKERBASQUE, 48013 Bilbao, Spain

6 ISIS Neutron and Muon Source, Didcot, UK

7 Institut Laue-Langevin, 71 Avenue Des Martyrs, Cedex 9 38042 Grenoble, France

8 Institute of Physics, University of Tartu, 50411 Tartu, Estonia

Published online: 18 April 2026

electrical functionality remains a key challenge for their wider implementation.

Recent reviews have summarized the state-of-the-art and future perspectives of UV-curable polymer-based smart materials, emphasizing their role in multifunctional applications and printed electronics [4]. Among the strategies to impart electrical conductivity, the incorporation of carbon-based nanofillers stands out due to their exceptional electrical, thermal, and mechanical properties [5, 6]. Carbon nanotubes (CNT) and reduced graphene oxide (rGO) are particularly promising because of their high aspect ratio, intrinsic conductivity, and ability to create percolated networks at relatively low concentrations [5, 7]. Beyond electrical conductivity, these fillers can introduce functional responses such as piezoresistivity, enabling strain or pressure sensing capabilities for wearables or structural health monitoring applications [8, 9], among others. Previous works, including UV-cured CNT/polyurethane acrylate composites for piezoresistive sensing [10] and bio-based AESO systems with conductive fillers [11], as well as more recent studies on carbonaceous composites with tunable piezoresistive response and multifunctional performance [12–15], have demonstrated the potential of nanocarbon-based UV-curable systems for sensing and flexible electronics applications. Furthermore, anisotropic architectures based on renewable resources have been explored for 3D-printed electrically conductive structures [16]. However, significant scientific and technological challenges remain. Achieving this goal demands an integrated approach that links materials selection and processing optimization to obtain proper processing-structure–property relationships, paving the way for the scalable fabrication of smart materials with tailored, application-specific functionalities.

The integration of CNTs and rGO into photocurable matrices is far from straightforward. Their strong optical absorption and visible light-scattering properties can limit photoinitiator activation and reduce UV penetration, leading to incomplete curing or heterogeneous crosslinking [17]. At the same time, the nanofiller–polymer interfaces may influence chain dynamics, mobility, and network development, with implications for mechanical and functional properties [18]. These factors make it essential to understand the interplay between filler type, content, and matrix characteristics during photopolymerization. While some studies have investigated functional characteristics of the composites, such as electrical conductivity or sensing performance [19, 20], comprehensive analyses that couple curing kinetics, structural dynamics, and multifunctional properties are scarce. Moreover, most previous works have focused on a single type of polymer matrix, often neglecting how the mechanical nature of the host material, i.e. elastic versus rigid, can modulate filler effects.

A key knowledge gap also lies in comparing CNT and rGO within UV curable composites prepared under identical experimental conditions. These two carbonaceous fillers exhibit distinct dimensionality, morphologies, aspect ratios, and surface chemistries. CNT, with their one-dimensional tubular structure and high UV absorption, typically achieve electrical percolation at lower concentrations but are more likely to inhibit radical polymerization [10, 17]. In contrast, rGO sheets present two-dimensional geometries with residual oxygen functionalities, favoring better dispersion and interfacial adhesion but requiring higher loadings to reach electrical conductivity thresholds [11, 21]. Despite their widespread use, systematic studies that address these aspects in parallel for elastic and rigid photocurable matrices, while exploiting advanced multiscale characterization techniques, are still limited.

In this context, the novelty of the present work does not rely on reporting record electrical conductivity or piezoresistive sensitivity, but rather on establishing a multiscale structure–processing–property framework for UV-curable carbonaceous composites. By combining real-time photorheology, quantitative nanostructural analysis by small-angle neutron scattering (SANS), polymer segmental dynamics probed by quasielastic neutron scattering (QENS), and macroscopic mechanical, electrical, and electromechanical characterization, this study elucidates how filler network archetype (1D CNT versus 2D rGO) and matrix mechanical nature (elastic versus rigid) jointly control curing efficiency, network heterogeneity, percolation behavior, and the sensitivity–stability trade-off in the piezoresistive response. This integrated approach enables the extraction of design-relevant insights that go beyond isolated structure–property correlations and provides guidance for the rational formulation of photocurable composites for sensing and multifunctional applications.

Therefore, this work investigates the influence of CNT and rGO incorporation on the photopolymerization behavior, molecular-level dynamics, and multifunctional properties of two UV-curable matrices with distinct mechanical characteristics: an elastic polyurethane acrylate (SPOT-E) and a rigid, bio-based acrylated epoxidized soybean oil (AESO). Curing kinetics was monitored to evaluate the effect of filler loading and type on gelation and crosslinking development while filler dispersion and aggregation were analyzed by scanning electron microscopy (SEM) and small-angle neutron scattering (SANS). To gain insight into polymer segmental mobility and polymer–filler interactions, quasielastic neutron scattering (QENS) was employed. Finally, mechanical characteristics, electrical conductivity, and piezoresistive response were assessed to establish correlations between nanoscale organization and macroscopic properties. By combining these multiscale analyses, this

study provides fundamental insights into how nanofiller morphology, content, and matrix characteristics control the multifunctionality of UV-curable composites, offering guidelines for their rational design of the materials for specific applications.

2 Results and discussion

2.1 Photocurable formulations

Before directly comparing CNT- and rGO-based composites, it is important to clarify that these two fillers are not intended to be evaluated as equivalent reinforcements at identical weight fractions. Due to their fundamentally different geometry, optical absorption, and aggregation behavior, CNT and rGO reach electrical percolation, viscosity build-up, and curing inhibition at markedly different filler contents. Therefore, comparisons throughout this work are performed in terms of relative network development rather than absolute filler loading. CNT and rGO are treated as two representative conductive network archetypes, namely entangled one-dimensional networks and stacked two-dimensional platelet networks, respectively, allowing to assess how filler geometry and matrix mechanical nature jointly influence curing behavior, nanoscale organization, and multifunctional performance.

First, the photopolymerization behavior of SPOT-E and AESO-based formulations containing CNT or rGO was investigated by real-time photorheology, monitoring the evolution of storage (G′) and loss (G″) moduli upon UV irradiation. This technique provides insights into both the kinetics of network formation and the viscoelastic transition from liquid-like to solid-like state, defined by the gel time (t_{gel}). Additionally, the initial slope of G′ versus time was used to estimate the curing rate ($\Delta G'/\Delta t$) [22], allowing quantitative comparison of formulation reactivity (Table S1, Supporting Information).

Figure 1 shows the evolution of G′ for SPOT-E and AESO composites as a function of time for different filler types and contents. Both neat matrices exhibit a nearly instantaneous onset of curing upon irradiation, characterized by a sharp increase in G′ and a rapid attainment of the plateau modulus, which reflects efficient crosslinking. The gelation time (t_{gel}) for pristine SPOT-E and AESO resins was 0.7 ± 0.3 s and 0.5 ± 0.1 s, respectively, confirming their high photoreactivity [10, 23].

The incorporation of nanocarbon fillers markedly influenced the curing behavior, as observed by the reduction in the slope of the G′ evolution curves and the decrease in final G′ values with increasing filler content, independently of the filler type and the matrix used. For CNT-based composites, increasing nanotube content significantly decreased $\Delta G'/\Delta t$ and extended t_{gel}, a behavior attributed to the strong UV absorption and light-scattering capability of CNT, which reduces the photon flux available for photoinitiator activation and subsequently hinders radical generation [17, 24]. As summarized in Table S1, the curing rate for SPOT-E decreased from 16.3 kPa/s for the neat resin to 0.088 kPa/s at 0.6 wt.% CNT, while t_{gel} increased from 0.7 s to 41.2 s. AESO-based materials exhibited a similar trend, with $\Delta G'/\Delta t$ decreasing from 15.9 kPa/s to 0.15 kPa/s and t_{gel} increasing from 0.5 s to 43 s over the same range of CNT loading. These observations are consistent with previous reports demonstrating that even small amount of CNT addition can dramatically inhibit UV curing due to optical shielding and radical quenching effects [10]. Furthermore, it is worth to mention that $\Delta G'/\Delta t$ decreases nearly of 185-fold in SPOT-E compared to 106-fold in AESO, suggesting that SPOT-E is more strongly affected by CNT in terms of curing rate inhibition. However, gelation delays are comparable in both systems (up to ~ 41–43 s), reflecting the similar optical screening effect of CNT at equivalent concentrations.

An even stronger impact on photopolymerization is observed for rGO-filled formulations, especially at the highest concentrations, as shown by the significantly low slopes of G′ curves in Fig. 1. SPOT-E shows a strong reduction in curing rate to 0.017 kPa/s at 5 wt.% rGO (959-fold decrease), whereas AESO decreases to 0.075 kPa/s (212-fold decrease) for the same filler content. At first glance, this suggests that SPOT-E is more sensitive to rGO in terms of curing rate, probably due to differences in photoinitiator concentration and light penetration in the commercial polyurethane acrylate matrix. However, it must be emphasized that rGO was incorporated at much higher concentrations (up to 5 wt.%), whereas CNTs could only be added up to 0.6 wt.% because higher loadings made complete curing impossible. Therefore, the more severe inhibition observed for rGO systems is partly a consequence of the larger filler content needed to approach electrical percolation. In contrast, gelation time is more affected in AESO-based materials, reaching 118 s at 5 wt.% rGO compared to 43 s for the SPOT-E-based sample, suggesting that the AESO/IBOMA blend experiences stronger network formation delays at high rGO loadings. This behavior can be attributed to the higher filler content required for rGO in AESO and possible strong interactions between rGO sheets and the bio-based matrix, which increase viscosity and hinder segmental mobility before gelation [11].

To further assess curing efficiency and complement the photorheology analysis, the degree of double-bond conversion was evaluated by transmission FTIR, as explained in the experimental section of Supporting Information. As shown in Table S1, the neat resins show high conversion

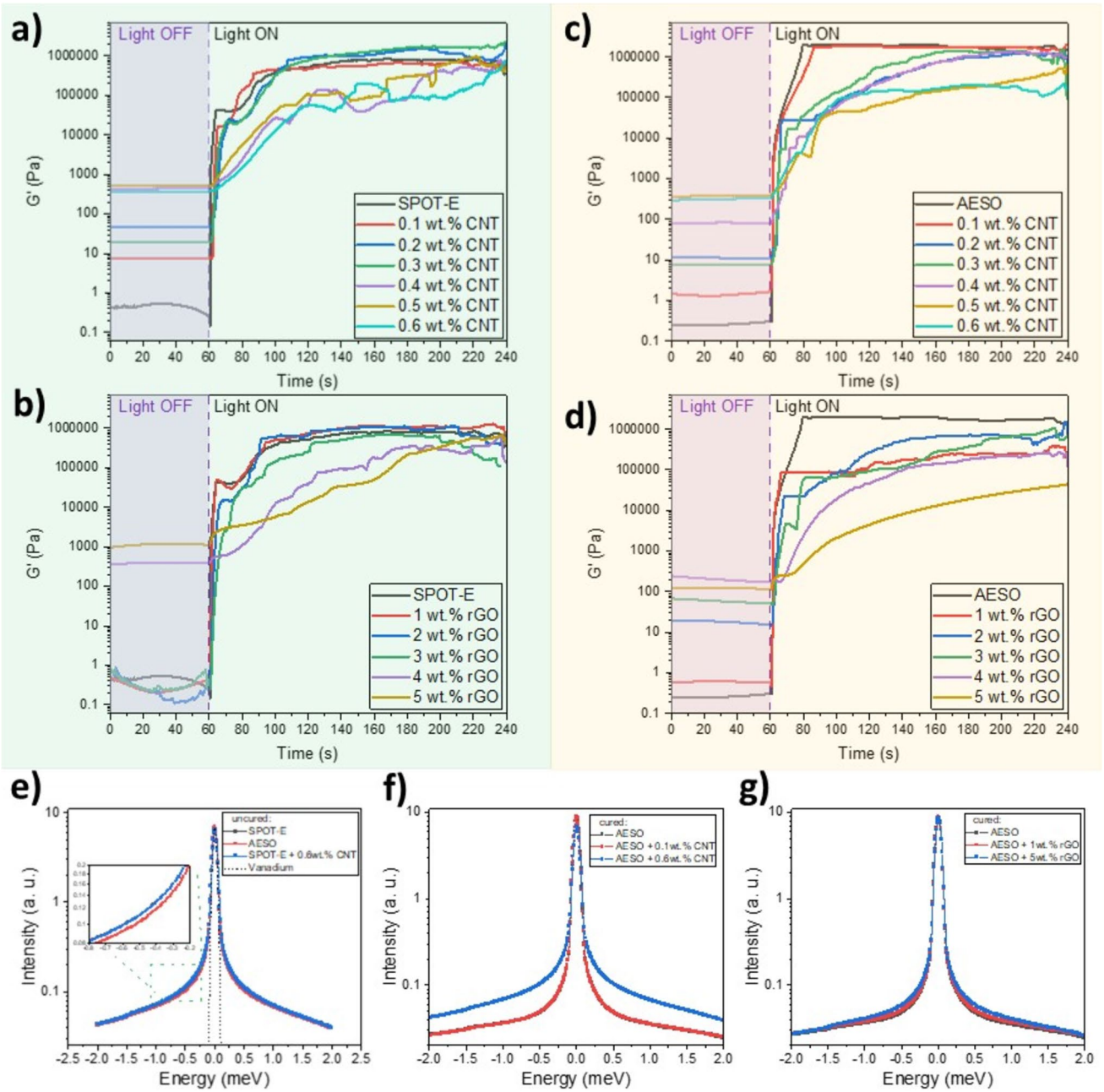

Fig. 1 Characterization of photocurable formulations: photorheology plots for the evolution of the storage modulus (G') of SPOT-E and AESO formulations containing CNT (**a** and **c**, respectively) and rGO (**b** and **d**, respectively). QENS spectra of uncured SPOT-E, AESO and SPOT-E + 0.6 wt.%CNT composite sample (**e**), cured AESO, AESO + 0.1wt.%CNT and AESO + 0.6wt.%CNT (**f**), and cured AESO, AESO + 1wt.%rGO and AESO + 5 wt.%rGO (**g**)

values around 80%, confirming efficient photopolymerization under the selected irradiation conditions. Upon incorporation of carbonaceous fillers, the conversion progressively decreases with increasing filler content in both matrices. This trend is particularly evident for CNT-containing formulations, where the presence of CNT networks reduces curing efficiency due to light attenuation, radical quenching, and restricted chain mobility. Conversions of samples with 0.1 wt.% CNT content are around 78% and 72% for SPOT-E and AESO-based materials, respectively, while for 0.3 wt.% CNT samples decrease to values of 70% and 63% being even less for the highest CNT content of 0.6 wt.% with minimal values of 55% and 47%, respectively. rGO-filled systems exhibit a similar but less pronounced decrease at intermediate concentrations, followed by a stronger reduction at high loadings (77%, 68% and 54% for 1, 3 and

5 wt.% SPOT-E/rGO samples, and 68%, 67% and 51% for the same rGO contents in AESO/rGO composites). These observations are consistent with the photorheology results, where increasing filler concentration leads to delayed gelation and reduced polymerization rate.

Overall, these findings confirm that both CNT and rGO act as inhibitors of photopolymerization, but their effects depend on the combination of filler type and resin matrix. CNT, with its tubular morphology and strong UV absorption, primarily reduces the polymerization rate at relatively low loadings, whereas rGO, despite requiring higher concentrations to achieve percolation, exerts a stronger effect on gelation delay in AESO-based systems. These trends are consistent with previous reports highlighting the dual role of nanocarbon fillers as optical screens and physical barriers that restrict chain dynamics during network formation [17, 25]. However, and in order to gain deeper understanding on the differences between both fillers and matrices in the photopolymerization process, QENS, a neutron scattering technique used to study the dynamics of materials at the atomic and molecular level, were performed and the results will be presented later in this section.

The rheological behavior of the uncured formulations was assessed through complex viscosity (η) measurements, providing critical information about their flowability, dispersion state, and suitability for UV-curable processing. Unlike steady-shear viscosity, complex viscosity determined under oscillatory conditions accounts for both viscous and elastic contributions to the response of the material, making it highly relevant for photopolymer systems intended for advanced manufacturing [26]. In particular, viscosity strongly influences light penetration and photoinitiator efficiency, as high viscosities can limit radical diffusion and restrict chain mobility during polymerization [27]. This aspect is especially critical in nanocomposite formulations containing carbonaceous fillers, since the addition of CNT or rGO typically increases viscosity due to their high aspect ratio and strong tendency to form interconnected networks [25]. Therefore, analyzing η as a function of filler type and concentration allows to understand how these nanofillers modify the processability of SPOT-E and AESO-based systems and anticipate their impact on curing kinetics and final material properties. Figure S1 and Table S1 (Supporting Information) summarizes the obtained η values.

For CNT-filled formulations, both SPOT-E and AESO matrices exhibited an evident viscosity increase with filler loading, but the magnitude of this effect is strongly matrix-dependent. The neat SPOT-E resin displayed a low η of approximately 0.28 Pa·s, confirming excellent flowability for coating and photopolymer applications. Incorporating CNT led to a moderate rise in viscosity at low contents, reaching 7.57 Pa·s at 0.3 wt.%, followed by a sharp increase for higher concentrations, ending at 90.4 Pa·s for 0.6 wt.% CNT filler content. AESO-based formulations showed a similar trend but started from a slightly higher baseline (1.06 Pa·s) and reached 114 Pa·s at the same maximum CNT content. This pronounced increase is attributed to the high aspect ratio (highly anisotropic shape) and strong van der Waals interactions of CNT, which promote early network formation and significant flow resistance even at sub-percent loadings [25]. Beyond a simple filler-loading effect, this progressive viscosity build-up reflects the development of an increasingly interconnected nanotube network within the resin, acting as an indirect rheological signature of network connectivity and structural organization. The more abrupt rise observed for SPOT-E suggests a stronger sensitivity of this commercial polyurethane acrylate resin to nanotube-induced structuring, possibly due to its lower initial viscosity and higher polarity compared to the AESO/IBOMA blend.

For rGO-filled systems, viscosity changes were even stronger, though it should be emphasized that rGO was incorporated at much higher loadings (up to 5 wt.%) compared to CNT. In SPOT-E, η increased progressively at intermediate concentrations but reached extremely high values at the highest rGO content (~441 Pa·s at 5 wt.%), representing a near-solid-like behavior that would severely compromise printability. AESO-based formulations followed a more gradual increase, remaining close to 60 Pa·s up to 3 wt.% and reaching 131 Pa·s at 5 wt.% rGO. The delayed viscosity buildup in AESO can be ascribed to the presence of IBOMA as reactive diluent, which lowers the effective concentration of rGO per unit volume and enhances dispersion at lower loadings [28]. Nonetheless, the substantial increase at 5 wt.% reflects the two-dimensional geometry of rGO and its ability to form extended sheet–sheet contacts, leading to significant microstructural hindrance of flow [29]. In contrast to the entangled CNT networks, the sharper viscosity rise at high rGO contents is consistent with the formation of contact-dominated platelet aggregates, indicating a different network architecture that can be correlated with the structural features observed by SEM and SANS.

Comparing both filler types, SPOT-E consistently exhibited greater sensitivity to viscosity rise than AESO, particularly at the highest rGO concentrations, where η values were more than three times higher for SPOT-E than for AESO under similar conditions. This outcome reinforces the stronger network-forming ability of CNTs and the higher structuring tendency of SPOT-E compared to the bio-based AESO/IBOMA system. However, when interpreting these results, it is crucial to consider that rGO was introduced at concentrations one order of magnitude higher than CNT, which naturally amplifies its impact on flow resistance. Taken together, these rheological signatures provide

indirect but valuable insight into filler network development and connectivity, complementing the nanoscale structural information obtained from SANS and the dynamic heterogeneity revealed by QENS. These findings emphasize the inherent trade-off between achieving electrical percolation and preserving acceptable rheological properties for UV-curable processing, as excessive viscosity not only compromises dispersion and coating uniformity but also hinders light penetration and radical mobility during photopolymerization [30].

Finally, correlating these trends with the photorheology results highlights a clear interplay between initial viscosity and curing behavior. Formulations with higher η exhibited more pronounced reductions in polymerization rate and significant delays in gelation, confirming that restricted chain mobility and increased optical attenuation in highly viscous dispersions aggravate the inhibitory effects of carbonaceous fillers. This relationship underscores the need for optimizing filler concentration and dispersion strategies to balance functional performance with processability.

In order to better understand the relationship between photopolymerization, molecular dynamics, and filler addition in SPOT-E and AESO systems, QENS experiments were conducted on both liquid and UV-cured states (Fig. 1). Since the neutron scattering signal is dominated by the incoherent component of the hydrogen atoms, QENS preferentially probes hydrogen dynamics and thus polymer matrix motions, providing insight into their underlying segmental mobility at picosecond-to-nanosecond timescales [31]. Unlike rheological or mechanical measurements, which provide macroscopic or mesoscale information, QENS enables the direct assessment of local chain dynamics and network heterogeneity arising from incomplete curing or filler-induced confinement effects. Therefore, QENS provides unique insight into how nanofillers modify polymer mobility at the molecular scale, complementing photorheology results and enabling a direct link between curing kinetics and nanoscale dynamic behavior.

In the uncured state, both SPOT-E and AESO exhibit pronounced quasielastic broadening, reflecting active translational and rotational motions [32, 33]. SPOT-E shows slightly faster dynamics than AESO, evidenced by an additional broadening near the elastic peak (–0.5 meV), consistent with its lower viscosity and higher segmental mobility prior to gelation. The incorporation of CNT or rGO does not significantly affect these liquid-state dynamics, as confirmed by the nearly overlapping spectra of SPOT-E and SPOT-E + 0.6 wt.% CNT in Fig. 1e. This observation suggests that in the absence of crosslinks, nanofillers exert minimal restrictions on short-range motions.

Upon UV curing, a substantial reduction in quasielastic broadening is observed for all samples, confirming the transition from mobile monomers to rigid crosslinked networks as it has been reported for related materials [34]. In SPOT-E-based systems, the cured state exhibits extremely restricted dynamics, and the addition of CNT or rGO does not noticeably alter this behavior, even at high filler contents, which aligns with the strong network rigidity inferred from rheological data. In contrast, AESO-based composites display a more complex scenario. While the neat AESO matrix becomes highly rigid after curing, the introduction of fillers modulates its dynamics depending on the filler type and concentration. At low CNT content, the QENS response remains comparable to that of neat AESO, indicating negligible changes in segmental mobility. However, at 0.6 wt.% CNT, a significant increase in mobility is detected, with the quasielastic intensity increasing to an intermediate level between fully cured and liquid AESO (Fig. 1f).This dynamics activation correlates with the extended gelation time and reduced curing rate observed in photorheology, suggesting that dense filler aggregates locally disrupt the network, generating regions of incomplete conversion and higher residual mobility.

rGO presents an even more pronounced effect on AESO dynamics (Fig. 1g). At 1 wt.% rGO, a slight increase in mobility is already detected and at higher loadings (5 wt.%), the effect becomes even more pronounced. Thus, probably the rigid, platelet-like nature of rGO, could favours filler stacking and induces stress concentration, hindering homogeneous network formation and leaving highly mobile domains.

Overall, QENS reveals that polymer segmental dynamics after curing are governed primarily by matrix chemistry, while being selectively modulated by filler-induced network heterogeneity. SPOT-E retains its rigid dynamic character regardless of filler type, ensuring mechanical robustness, whereas AESO exhibits partial recovery of mobility at high filler contents, consistent with its lower effective crosslink density and heterogeneous network structure. Importantly, these nanoscale mobility variations, directly captured by QENS, complement rheological observations and provide molecular-level evidence of curing inhibition and heterogeneity that cannot be resolved by macroscopic techniques alone, helping to rationalize the observed differences in mechanical and electromechanical performance.

2.2 Photocured materials

2.2.1 Physico-chemical and morphological characteristics

The chemical structure of the photocured composites was analyzed by FTIR-ATR spectroscopy to evaluate possible physicochemical interactions between nanofillers and the polymer matrix and to detect residual functional groups

after UV curing. FTIR is a suitable technique for identifying characteristic vibrational bands associated with acrylate networks and potential filler-induced effects. For both SPOT-E- and AESO-based materials, the spectra (Fig. 2) are dominated by the typical polymer backbone vibrations. In the case of SPOT-E (a polyurethane acrylate resin), the main absorption bands appear at 3330–3400 cm^{-1} (N–H stretching), 2855–2955 cm^{-1} (CH_2 and CH_3 stretching), 1725 cm^{-1} (C=O stretching), 1550 cm^{-1} (combined N–H and C–N stretching), 1360 cm^{-1} (C–N stretching), and 1110 cm^{-1} (C–O–C stretching)[10]. For AESO-based systems, the spectra exhibit bands at 3460 cm^{-1} (-OH stretching), 1730 cm^{-1} (C=O stretching of ester groups), and 1160 cm^{-1} (C–O–C vibrations), together with peaks associated with the triglyceride backbone at 2920, 2850, and 1450 cm^{-1} (C–H stretching and deformation). Additionally, the acrylic double bond functionality is represented by absorptions near 1635 cm^{-1} and 810 cm^{-1} [11].

The incorporation of CNT or rGO introduces two clear features: (i) increased noise in the carbonyl region (≈1700 cm^{-1}), likely associated with scattering effects from nanofillers[35, 36], and (ii) the appearance or intensification of the band at ~810 cm^{-1}, attributed to out-of-plane bending of residual vinyl groups (C=C), which becomes more evident as the filler content increases, regardless of the filler type or matrix. This observation suggests that at high nanofiller loadings, a fraction of acrylate double bonds remains unreacted, most likely due to reduced UV penetration and restricted mobility during network formation [37]. These results are consistent with the curing inhibition trends previously identified by photorheology and viscosity analyses.

The presence of residual C=C signals is more pronounced in composites with higher filler loadings, which correlates with the optical shielding and increased viscosity discussed earlier. For CNT-containing systems, the effect is observed at relatively low concentrations (≥0.3 wt.%), whereas in rGO-based composites, noticeable residual unsaturation appears primarily at 1 wt.%. This difference can be attributed to the distinct morphologies and percolation behaviors of the fillers: the 1D structure of CNT creates strong light attenuation and network constraints even at low loadings, while 2D rGO requires higher contents to produce comparable effects. Moreover, AESO-based formulations tend to show slightly more evident vinyl-related bands

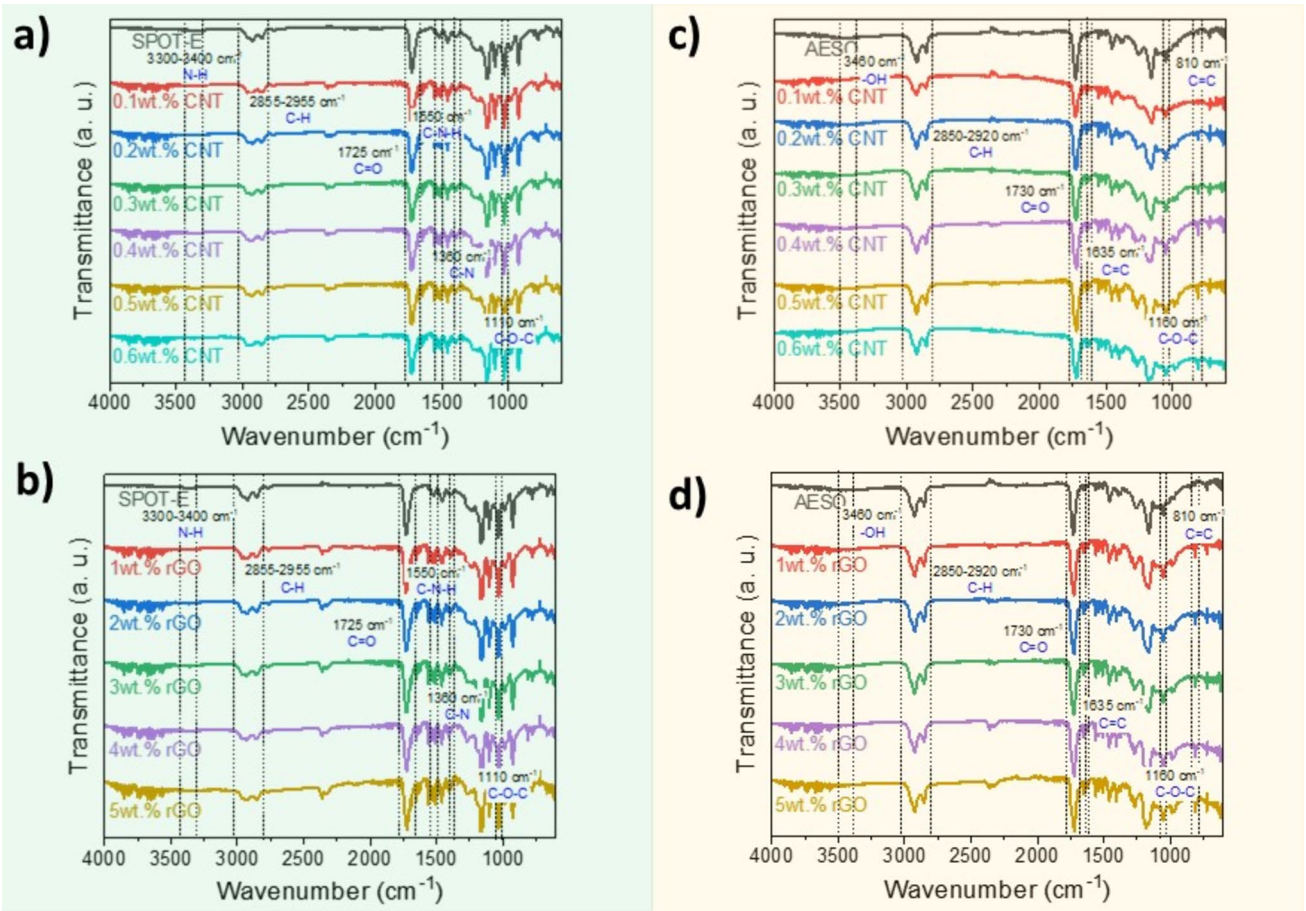

Fig. 2 FTIR plots for SPOT-E and AESO photocured materials containing CNT (**a** and **c**, respectively) and rGO (**b** and **d**, respectively)

than SPOT-E at equivalent filler conditions, suggesting that the bio-based matrix, despite being diluted with IBOMA, is more susceptible to incomplete double bond conversion under high filler contents. These observations reinforce the relationship between filler concentration, viscosity increase, and limited UV curing efficiency, in agreement with the rheological findings.

Filler dispersion and wettability between the CNT and rGO, and the SPOT-E and AESO polymer matrices were evaluated by SEM images analysis of thin film samples with different filler contents. Figure 3 shows representative SEM images of pristine and reinforced composites at different magnifications revealing significant differences in filler dispersion and microstructural organization as a function of filler type, concentration, and polymer matrix. Pristine AESO and SPOT-E films exhibit smooth, homogeneous fracture surfaces without voids or irregularities, indicative of fully crosslinked and defect-free matrices. Upon incorporation of nanocarbonaceous fillers, the morphology changes markedly.

For CNT-based composites, both AESO and SPOT-E matrices display an overall good distribution of nanotubes at low concentrations (0.1 wt.%), with no evidence of large aggregates or interfacial gaps. The polymer appears to wet the nanotubes efficiently, forming a continuous phase without microvoids. At higher contents (0.4 and 0.6 wt.%), localized clusters of CNT become evident. Based on SEM observations, these agglomerates are estimated to fall predominantly within the ~ 1–20 µm range, with occasional clusters approaching ~ 30 µm. These clusters are homogeneously distributed throughout the matrix, which is beneficial for electrical percolation but could affect mechanical properties by creating local stress concentrations. This morphology correlates with rheological behavior, as CNT entanglements enhance viscosity and contribute to curing delays (Sect. 3.1). Similar trends were reported for UV-curable polyurethane acrylate/CNT systems, where effective dispersion combined with some clustering was associated with enhanced electrical conductivity at the expense of toughness [10]. Consistent with this morphology, CNT-based

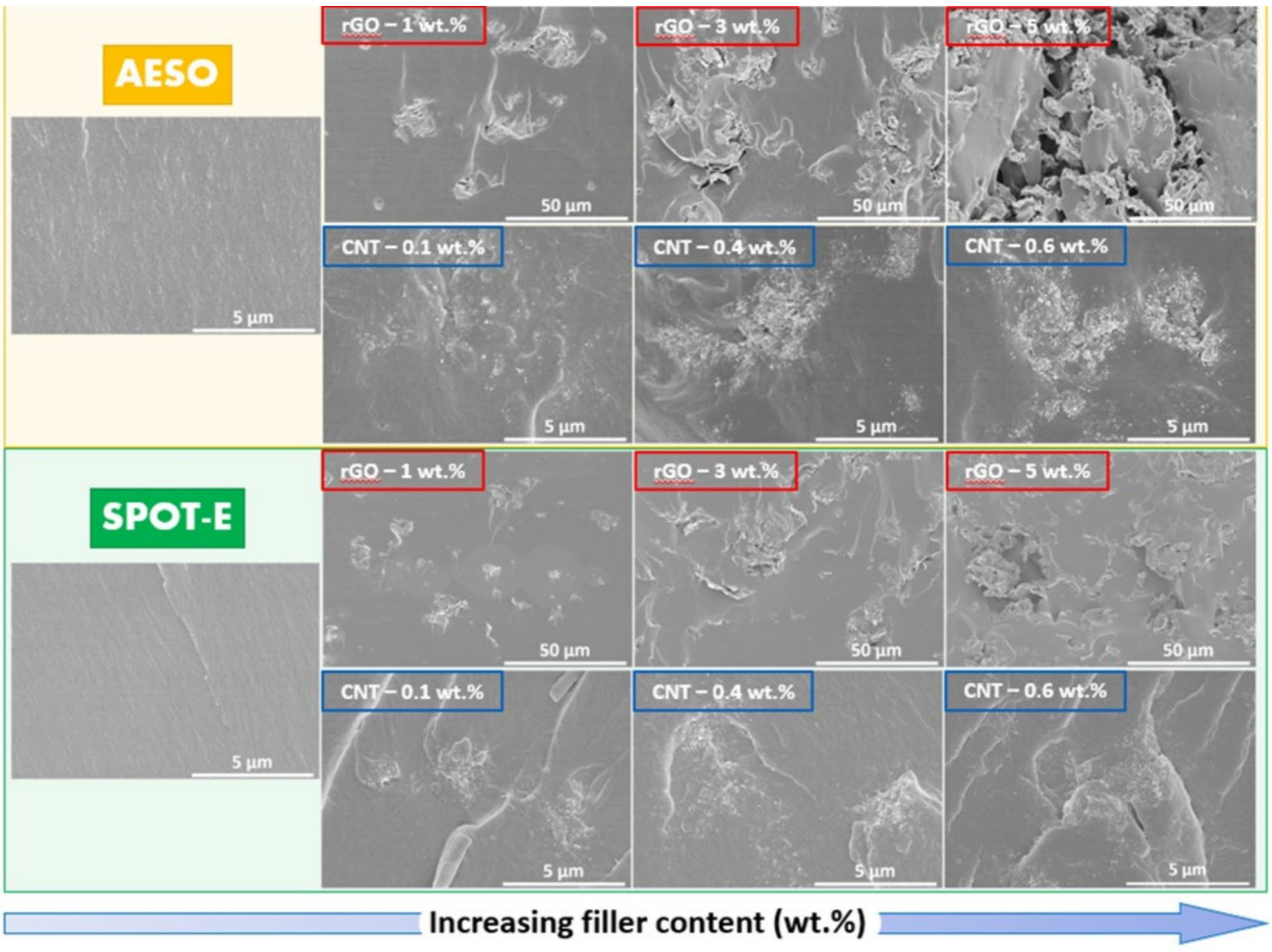

Fig. 3 SEM images of pristine and doped samples containing rGO and CNT for AESO (top) and SPOT-E (bottom) composites. Magnification for neat polymers and CNT containing sample is 5000 × and for rGO-based materials is 1000 ×

systems reach electrical percolation at relatively low loadings (~0.28–0.30 wt.%) as it will be shown later, indicating that interconnected nanotube clusters provide efficient conductive pathways even at limited filler concentrations.

For rGO-based composites, the presence of graphene platelets is clearly observed as bright, flake-like structures embedded within the polymer matrix. At 1 wt.% rGO, the AESO and SPOT-E films show well-dispersed small clusters, but as the filler content increases to 3 and 5 wt.%, larger agglomerates dominate the morphology, forming stacked structures with irregular shapes and limited polymer penetration. From SEM micrographs, the characteristic lateral size of these rGO aggregates is estimated to increase from roughly ~ 10–20 µm at low loadings to approximately ~ 30–80 µm for the highest filler concentrations. Despite this aggregation, the fillers remain relatively well distributed at the microscale, with no extensive phase separation. However, samples containing 5 wt% rGO exhibit microvoids and interfacial gaps, particularly in AESO, likely due to the increased viscosity and restricted flow during processing, as previously noted in photorheology and viscosity analyses. These voids could negatively impact mechanical integrity while promoting pathways for electrical conduction. Across both filler types, AESO generally shows slightly larger, more compact agglomerates and occasional microvoids at the highest loadings (notably 5 wt% rGO) than SPOT-E, whose fracture surfaces remain more uniformly wetted with fewer interfacial gaps. This microstructural organization is consistent with the higher filler concentrations required for electrical percolation in rGO systems, where conductive pathways are primarily established through platelet stacking and inter-aggregate contacts.

A suitable distribution of small agglomerates, rather than isolated particles, is considered advantageous for building conductive networks in nanocomposites [38], although excessive clustering and void formation can compromise toughness and optical quality. Electrically, the presence of well-distributed micro-sized clusters in both matrices is favorable for forming percolated pathways, with rGO stacks facilitating conduction at higher contents and CNT entanglements enabling pathways at lower contents. Mechanically, the cleaner interfaces and lower void density in SPOT-E should better preserve toughness and elongation, while the voids and sharper rGO stacks observed in AESO at 5 wt% are likely to act as stress concentrators, contributing to earlier damage onset and a steeper decline in ductility (trends consistent with the photorheology-indicated network development and the viscosity-limited flow during curing). These SEM findings will be correlated with mechanical characteristics and electrical conductivity, later explained, to provide a comprehensive structure–property analysis.

While SEM provides valuable information on micron-scale dispersion and fracture morphology, it cannot resolve the nanoscale organization and connectivity of conductive filler networks that govern electrical percolation and polymer–filler interfacial interactions. Therefore, small-angle neutron scattering (SANS) was employed to quantitatively investigate the nanostructural organization of CNT and rGO within SPOT-E and AESO matrices. Due to the strong scattering length density contrast between carbonaceous fillers and hydrogen-rich polymer matrices, SANS enables the extraction of aggregate fractal descriptors, filler characteristic dimensions, and packing density, providing quantitative information on network architecture that is inaccessible through microscopy alone.

Figure 4 displays the SANS profiles of SPOT-E and AESO composites as a function of filler type and content, plotted as scattering intensity, I, versus scattering vector, q. In these nanocomposites, the main scattering contribution arises from the carbonaceous fillers due to the strong scattering length density (SLD) contrast between carbon materials and the surrounding hydrogen containing polymer matrix [39]. All filled samples exhibit one power-law decay (in the low q-region for CNT filler and in almost all q-region studied for rGO), confirming the formation of fractal-like aggregates [40], whereas the neat polymers show almost negligible scattering, confirming homogeneity of the matrix without nanoscale inhomogeneity in pure polymer films.

For CNT-based systems, an additional scattering signal is observed for high q values, corresponding well to cylinder form-factor in the scattering objects. This agrees with the samples measured, as CNT are characterized by a cylindric shape. For all samples, independently of the CNT content and the matrix studied, the scattering cylinders can be well fitted with a radius of 60 Å (diameter ≈12 nm), what is in agreement with the technical data given by the supplier for the CNT. The slopes observed for CNT-filled samples correspond to power exponents values below 3 in all cases regardless the filler content and polymer matrix used, suggesting that all CNT-based composites exhibit mass fractal-like aggregations [41]. While for both SPOT-E and AESO-samples at low CNT contents the power exponent is similar and ~ 2.4, the addition of CNT induces different behaviour for each polymer matrix. On the one hand, for the elastic polyurethane acrylate SPOT-E matrix, the q exponent is maintained almost constant for all contents studied, indicating that the addition of CNT increases the number of aggregates, but their characteristic size and type of aggregation are constant. On the other hand, the bio-based and more rigid AESO matrix presents an increase of power exponent when CNT content increases reaching a maximum of ~ 2.7 for 0.6wt.% sample, which indicates some structural reorganization of the CNTs aggregates, namely a denser

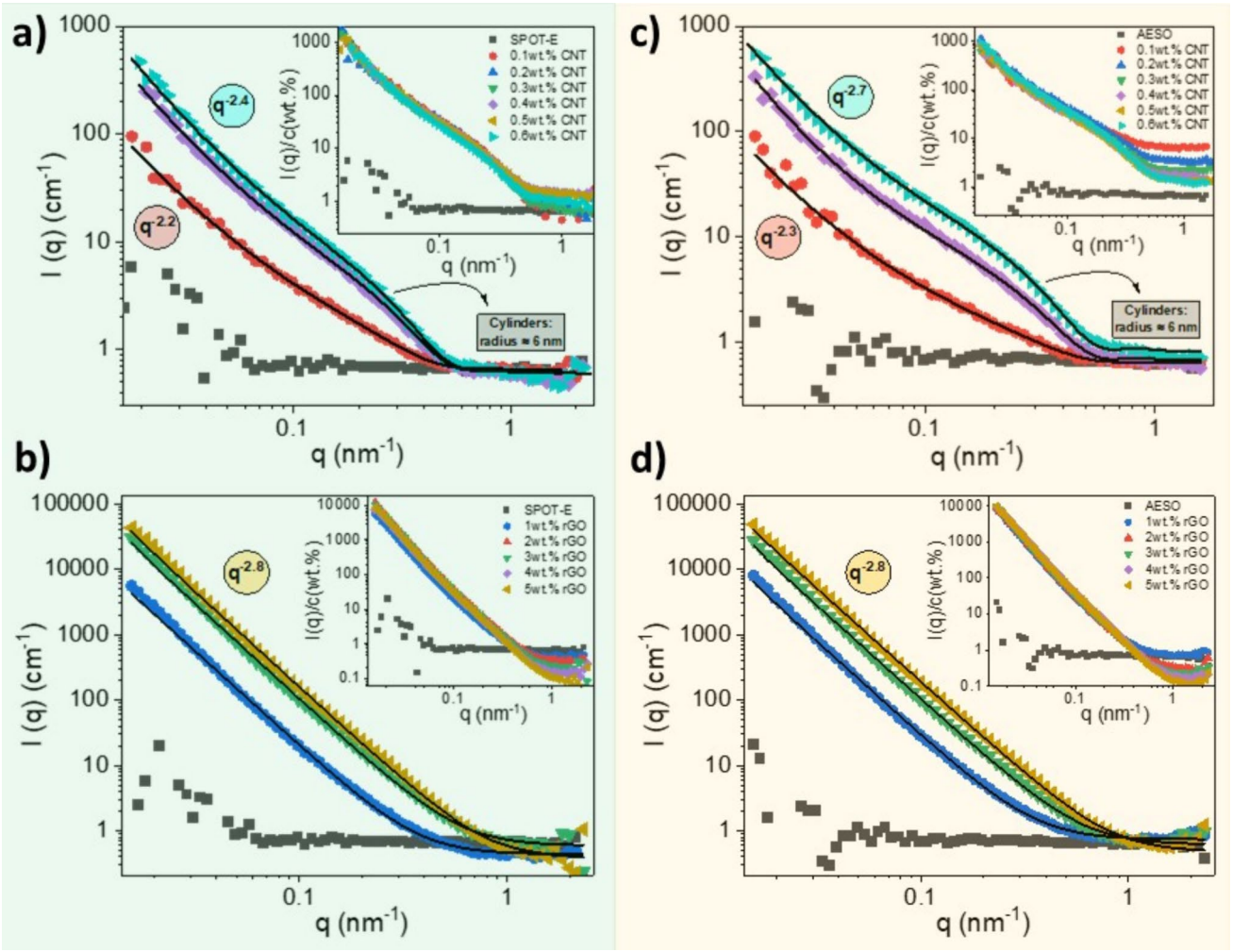

Fig. 4 Experimental SANS plots for pristine and SPOT-E and AESO composites containing CNT (**a** and **c**, respectively) and rGO (**b** and **d**, respectively). Inset figures of (**a**–**d**) plot the SANS curves normalized to the filler content. Solid lines indicate the power law (and cylindrical in case of CNT) fit with corresponding exponent values

packing of the aggregates when CNTs are added [40, 42]. These higher exponents observed in AESO-based materials suggest stronger inter-filler interactions and less polymer penetration compared to SPOT-E-based composites, in agreement with SEM evidence of compact agglomerates and occasional voids at high loadings.

For rGO composites, both matrices display a single dominant slope close to ~ 2.8 across the measured q range, indicative of mass fractal aggregates denser than the ones of CNT-based composites and significant packing density [43–45]. These trends reflect the intrinsic differences in filler geometry (rigid platelets vs entangled nanotubes) and the influence of matrix chemistry on aggregation mechanisms, also mentioned and discussed in relation to the SEM results.

Furthermore, these nanoscale features explain the differences observed in rheology and curing behavior: in AESO, the presence of denser and more compact aggregates (especially for CNT at high contents and for rGO stacks) tends to restrict local mobility and contributes to longer gelation times. In contrast, SPOT-E develops more open and branched structures, which allow better polymer penetration and promote faster network formation despite still achieving electrical percolation at relatively low filler contents (see electrical results). However, and as previously mentioned, when considering the relative increase with respect to the neat resin, SPOT-E shows greater sensitivity to viscosity rise than AESO, particularly at the highest rGO concentrations, where η values become more than three times higher for SPOT-E. This is attributed to SPOT-E's much lower initial viscosity, making the same filler-induced network formation more impactful on flow resistance compared to the inherently more viscous AESO system. From a mechanical standpoint (results show in the following), the tightly packed rGO stacks and occasional voids observed in AESO are likely to act as stress concentrators, reducing toughness. SPOT-E, on the other hand, benefits from better wetting of

CNTs and less compact aggregates, which should help preserve ductility and mitigate premature failure.

Overall, SANS confirms that the fractal organization of carbon nanofillers depends strongly on both filler type and matrix polarity, complementing SEM observations and providing a nanoscale rationale for the differences in curing kinetics and viscosity response analyzed in previous sections but also for mechanical and electrical performance, as it will be show in the following.

2.3 Mechanical and electrical properties

The influence of filler addition and dispersion on the mechanical properties was evaluated by strain–stress measurements of thin film samples with different filler contents. Figure 5 shows representative stress–strain curves of the investigated samples, and Table S2 (Supporting Information) summarized the Young modulus (E), stress at break (σ_b) and strain at break (ε_b) values.

For SPOT-E-based composites, the neat matrix exhibited a soft and highly extensible behavior (E ≈ 6.8 MPa, ε_b ≈ 35.7%), typical of flexible polyurethane acrylates. Incorporation of CNT led to a progressive decrease in ductility, with ε_b dropping below 20% for 0.3 wt.% CNT composites, accompanied by a reduction in σ_b to 0.98 MPa. Interestingly, Young modulus (E) remained relatively stable up to 0.2 wt.% CNT but decreased at higher loadings, reflecting the detrimental effect of microsize agglomerates observed in SEM, which act as stress concentrators and promote premature failure[46]. The presence of rGO further accentuated this trend: while 1 wt.% rGO maintained moderate extensibility (ε_b ≈ 26.6%), higher concentrations resulted in severe embrittlement, with ε_b falling to 5.4% and σ_b to 0.04 MPa at 5 wt.% filler content. These mechanical degradations align with photorheology results, where high rGO content significantly delayed gelation and reduced curing efficiency, likely leading to a lower crosslink density and weak interfacial adhesion [11, 47].

AESO-based systems, inherently stiffer (E ≈ 230 MPa), displayed an opposite initial trend: the addition of 0.1 wt.% CNT slightly increased σ_b from 8.9 MPa to 10.1 MPa and enhanced ductility to 11% starting from 7.6%, suggesting improved stress transfer at low filler contents due to better dispersion of the filler and thus easy incorporation into the polymer matrix. However, for samples with higher CNT contents, all mechanical parameters deteriorated sharply, with E dropping below 12 MPa and σ_b to 0.75 MPa at 0.4 wt.% CNT, correlating with CNT clustering and viscosity-driven processing issues explained before. For rGO-filled AESO composites, 1 wt.% preserved stiffness and strength close to the neat resin, but concentrations equal or larger than 2 wt.% caused a drastic decrease in E (≈19 MPa) and σ_b, and at 5 wt.% rGO the material exhibited the lowest elongation (ε_b ≈ 3.3%), consistent with void formation and stacked platelet aggregates observed in SEM.

Comparing both matrices, SPOT-E maintains flexibility even at moderate filler contents, whereas AESO suffers a more pronounced stiffness decrease and embrittlement at high loadings. This contrast reflects their different network architectures and curing behavior: AESO, being highly crosslinked in the pristine state, is more sensitive to curing inhibition and morphological defects introduced by fillers. These mechanical trends also parallel electrical and rheological observations: while clustering favors conductive network formation, it compromises mechanical integrity [48], particularly in AESO with rGO at 5 wt.%, where poor wetting and sharp aggregates act as crack initiation sites. Further nanostructural insights from SANS confirm that the nanoscale organization of fillers largely governs this balance between conductivity and mechanical robustness. It is worth noting that, even at the highest filler concentrations where elongation is reduced, the strain levels remain sufficient for piezoresistive sensing applications, where only small deformations (typically below 5%) are required to achieve a measurable electrical response variation [49]. Although high filler loadings, particularly in AESO-based systems, lead to marked reductions in tensile strength and modulus, the absolute mechanical values remain compatible with low-strain sensing applications within the intended operating window [49]. Nevertheless, the mechanical deterioration observed at elevated CNT and rGO contents highlights the need for formulation optimization.

The electrical characteristics of the composites were evaluated by measuring the DC electrical conductivity as a function of nanofiller content. Figure 5e and f shows the variation of electrical conductivity (σ) for the photocured films, while the corresponding values are summarized in Table S2. To account for the intrinsic differences in percolation thresholds and processing windows between CNT and rGO systems, structure–property relationships are interpreted relative to the development of conductive networks, i.e., at loadings close to or above the respective percolation thresholds, rather than at identical filler contents. This approach enables a more meaningful comparison of electrical and electromechanical behavior across different filler types and polymer matrices.

In case of CNT-based composites, both matrices exhibit a percolation-type behavior, with conductivity remaining close to that of the insulating polymer at very low nanotube concentrations and then increasing dramatically upon reaching the critical threshold. For SPOT-E composites, electrical conductivity rises from 1.2×10^{-11} S/m for the neat matrix to 2.9×10^{-7} S/m at only 0.1 wt.% CNT, marking the onset of electrical percolation. A sharp growth follows between 0.2

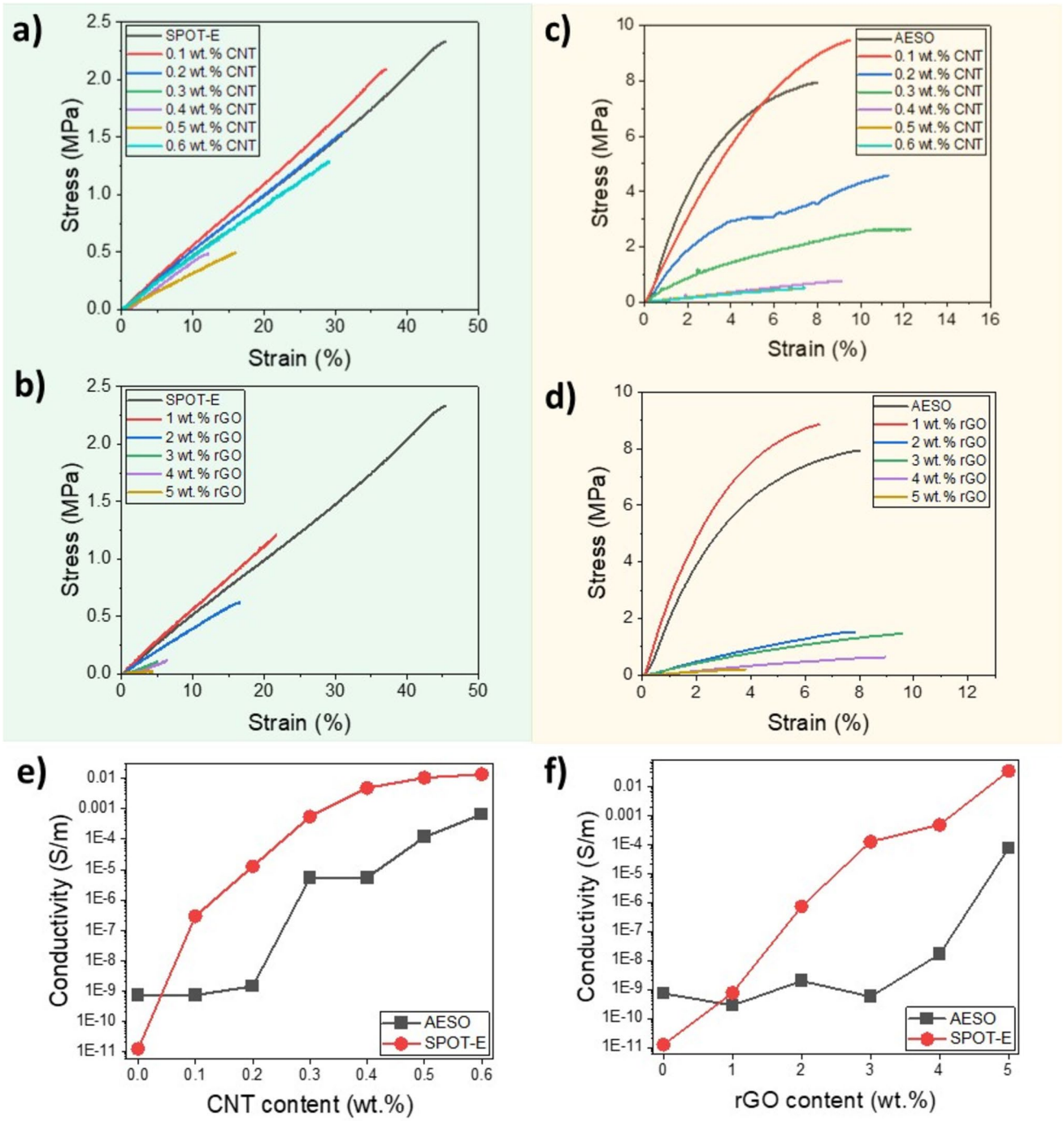

Fig. 5 Mechanical and electrical characterizations: stress–strain curves of solid photocured specimens for SPOT-E and AESO composites with CNT (**a** and **c**, respectively) and rGO (**b** and **d**, respectively). Electrical conductivity as a function of CNT (**e**) and rGO (**f**) content for the prepared composites

wt.% and 0.4 wt.% (1.3×10^{-5} to 4.9×10^{-3} S/m), reaching 1.4×10^{-2} S/m at 0.6 wt.%, where an interconnected CNT network is fully developed. In contrast, AESO-based composites require higher filler contents to achieve significant conductivity gains. Up to 0.2 wt.% CNT, the conductivity remains below 4.9×10^{-9} S/m, and only at 0.3 wt.% a noticeable increase appears (5.4×10^{-6} S/m), continuing to rise more gradually than in SPOT-E and reaching 6.9×10^{-4} S/m at 0.6 wt.%. This difference in percolation dynamics correlates with the morphological features observed by SEM and SANS: the more open and branched CNT networks formed in SPOT-E facilitate early percolation, while

AESO's denser and less interconnected clusters, combined with high viscosity, hinder network continuity at low loadings. These trends are consistent with previous reports on UV-curable nanocomposites where CNT dispersion quality and matrix polarity strongly influence percolation thresholds [10, 50, 51]. In these works, similar tendency of increasing conductivity with CNT incorporation is obtained with a final value of 7.1×10^{-2} S/m for the same 0.6 wt.% CNT content reported in the present study.

Regarding rGO-based composites, σ evolution for graphene-filled systems differs markedly from that of CNT composites. For SPOT-E, rGO begins to significantly influence conductivity only at contents ≥ 2 wt.%, where values rise from the baseline (1.2×10^{-11} S/m) to 7.3×10^{-7} S/m, and then sharply increase to 1.3×10^{-4} S/m at 3 wt.% and 3.5×10^{-2} S/m at 5 wt.%. AESO follows a similar pattern but with slightly lower conductivity across the range, reaching 7.5×10^{-5} S/m at 5 wt.%. The delayed percolation and lower conductivity compared to CNT-based systems stem from the different filler morphology: rGO platelets show lower aspect ratio than CNT and tend to stack and form compact aggregates, as shown in SEM and SANS analyses, requiring higher contents to achieve continuous conductive paths [52]. Additionally, rGO's optical absorption and influence on curing may further restrict the formation of well-integrated conductive networks within AESO [11, 53], which is more susceptible to photopolymerization inhibition than SPOT-E as previously explained.

Comparing both filler types and matrices reveals that CNT systems outperform rGO systems in achieving high conductivity at lower loadings, particularly in SPOT-E, where percolation occurs at low filler contents (≈0.2/0.3 wt.%) and σ surpasses 10^{-2} S/m at 0.6 wt.%. For rGO, even at 5 wt.%, conductivity remains lower than SPOT-E + 0.6 wt.% CNT, confirming that entangled CNT networks provide superior connectivity per unit of weight compared to stacked graphene platelets, as reported in literature [54, 55]. These electrical trends align with rheological and mechanical observations. Furthermore, the reduced conductivity of AESO-based samples at equivalent filler contents is consistent with its higher tendency toward dense filler packing and interfacial defects, which also negatively affect mechanical characteristics. These interrelations underscore the inherent trade-off between achieving electrical functionality and maintaining processability and structural integrity.

A quantitative percolation analysis was performed to further evaluate conductive network formation. The corresponding log–log percolation fits and fitting ranges are provided in Figure S2 (Supporting Information). CNT-based systems exhibit low percolation thresholds, with filler concentration at the percolation threshold (φ_c) ≈ 0.28 wt.% for SPOT-E and ≈ 0.30 wt.% for AESO, confirming the efficient network-forming capability of high-aspect-ratio nanotubes at sub-percent loadings. In contrast, rGO-based composites require significantly higher filler contents to achieve electrical continuity, with $\varphi_c \approx 2.18$ wt.% for SPOT-E and $\varphi_c > 3$ wt.% for AESO within the investigated range, reflecting the platelet morphology and stacking tendency of rGO. The extracted critical exponents (t) range from 1.24 for SPOT-E/CNT to higher values for AESO/CNT and rGO-based systems, indicating sharper percolation behavior in CNT networks and broader, more contact-dominated transitions in platelet-based rGO composites [5, 56]. Overall, these percolation parameters are fully consistent with the conductivity evolution, rheological response, and morphological features discussed above.

2.3.1 Piezoresistive response

Considering the combined overall properties of composites, two representative samples were selected for electromechanical evaluation: SPOT-E with 0.6 wt.% CNT, offering high conductivity and suitable flexibility, and AESO with 5 wt.% rGO, corresponding to the maximum achievable conductivity for graphene-based composites under the processing constraints of these formulations. Both systems were selected above their respective percolation thresholds to ensure stable conductive pathways under mechanical stimulus, to evaluate their piezoresistive sensitivity. As commonly reported for nanocarbon-filled polymers [57, 58], composites near or slightly above percolation exhibit the highest sensitivity due to tunneling and microcrack-induced modulation of conductive networks, although large strains may cause irreversible network disruption [59]. Accordingly, a deformation range of 0.5–5% was adopted to evaluate sensor-relevant performance under controlled cyclic loading. Thus, the electromechanical response of these materials was characterized under uniaxial tensile loading while simultaneously monitoring electrical resistance. Figure 6 shows the relative resistance change ($\Delta R/R_0$) as a function of applied strain (ε) for both composites, together with the linear gauge factor (GF) calculation and the corresponding GF values.

In the case of SPOT-E + 0.6 wt.% CNT, the relative resistance variations follow the applied strain cycles with high repeatability and small baseline drift, confirming the mechanical stability of the conductive network [60]. The response remains monotonic with applied strain, mainly in load cycles. However, the GF remains below unity across the tested strain range, exhibiting an increase from approximately GF ≈ 0.4 at 0.5% strain to GF ≈ 0.9 at 5% strain. GF values below 1 are characteristic of robust percolated CNT networks with moderate variations compared to percolation near the threshold. This behavior aligns with the good interfacial bonding and flexible nature of SPOT-E, which

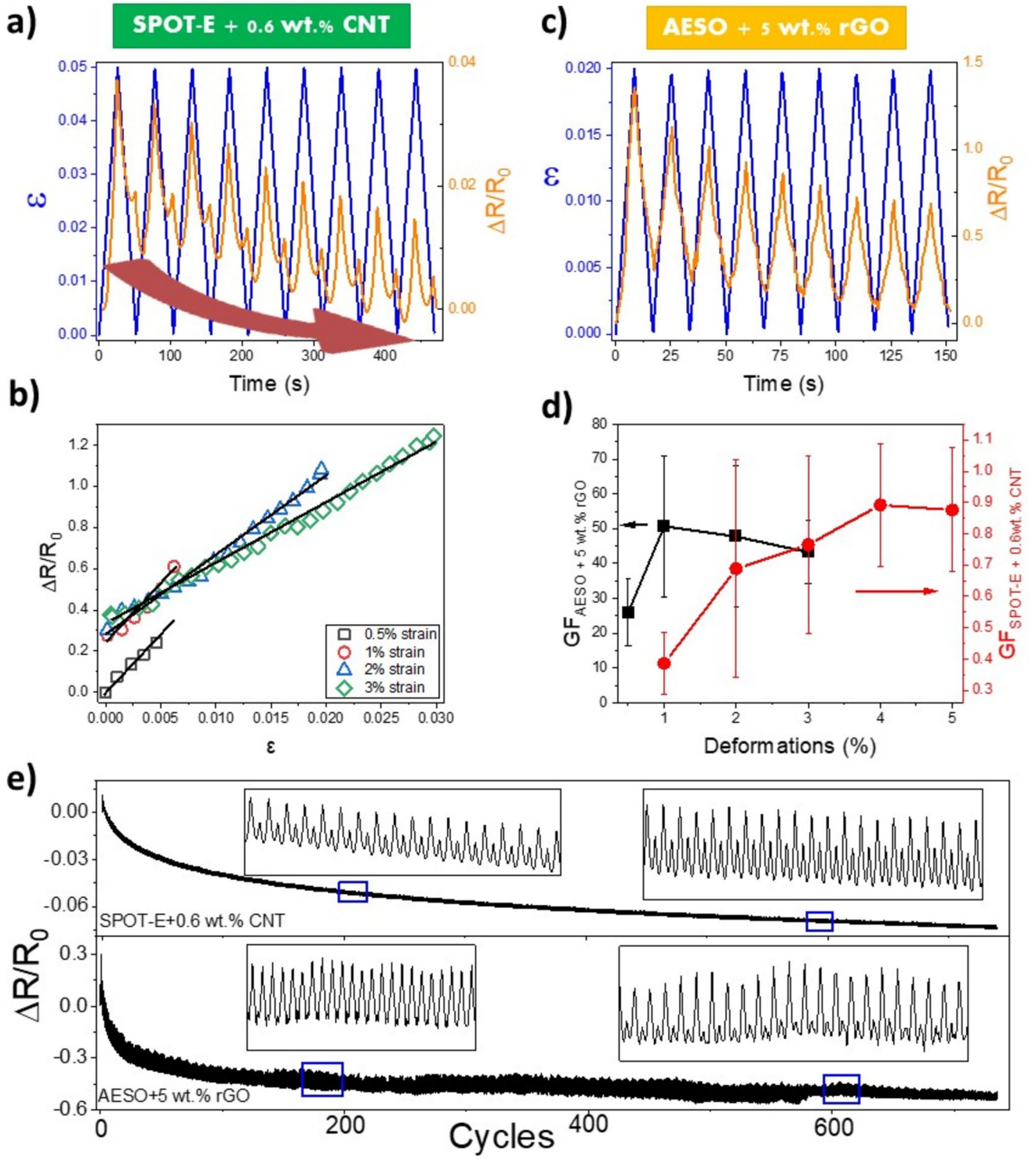

Fig. 6 Electro-mechanical properties of SPOT-E + 0.6 wt.% CNT composite at 5% strain (**a**) and AESO + 5 wt.% rGO sample at 2% strain (**c**). Illustration of GF calculation for AESO + 5 wt.% rGO sample at 0.5, 1, 2 and 3% strains (**b**). Piezoresistive sensibility (GF values) as a function of the strain deformations in % for both studied composites (**d**). Cyclic piezoresistive stability of SPOT-E + 0.6 wt.% CNT composite and AESO + 5 wt.% rGO sample under 1% strain (1 mm/min) for ~ 700 loading–unloading cycles (**e**)

limit microcrack formation and large tunneling gap variations under strain, thereby favoring durability over extreme sensitivity [61].

In contrast, AESO/rGO composite exhibits $\Delta R/R_0$ responses up to two orders of magnitude higher than SPOT-E/CNT for similar strains, with GF around 50 at 3% strain and despite its lower electrical conductivity. This is a consequence of their weaker and more brittle conductive network formed by stacked rGO platelets, exhibiting large variations under applied strain. Even though the AESO matrix is more rigid, composite present higher sensitivity to deformation-induced separation (stacked rGO platelets undergoes pronounced disruption under tensile loading, increasing interparticle distances and reducing contact points) [62, 63]. The nearly linear relationship between $\Delta R/R_0$ and strain suggests that GF remains relatively stable across the strain range, though local voids and microcracks (previously evidenced by SEM) likely contribute to higher noise and irreversible changes during prolonged cycling [64].

To evaluate long-term electromechanical stability, cyclic piezoresistive tests were performed at 1% strain and 1 mm/min for approximately 700 loading–unloading cycles (Fig. 6e). SPOT-E/CNT composites exhibit highly stable resistance responses, with only a slight progressive decrease in baseline resistance and nearly constant minimum and maximum resistance values per cycle, confirming good signal repeatability and mechanical durability. In contrast, AESO/rGO composites show an initial decrease in electrical resistance during the first ~ 50–60 cycles, followed by stabilization over the remaining cycles. This initial conditioning effect is attributed to microstructural rearrangement of the conductive network under repeated strain. After stabilization, the piezoresistive response remains reproducible, indicating that despite the higher sensitivity of AESO/rGO systems, acceptable cyclic stability can be achieved. Nevertheless, AESO/rGO composites exhibit slightly higher hysteresis and baseline drift compared to SPOT-E/CNT, consistent with microstructural rearrangement and limited interfacial debonding within the stiffer matrix and more compact platelet aggregates. These results confirm the distinct stability-sensitivity trade-off identified for the two matrix–filler combinations.

The electrical conductivity and piezoresistive performance obtained in this study are consistent with previously reported UV-curable CNT- and graphene-based composites [65, 66]. UV-cured CNT/polyurethane acrylate systems typically exhibit gauge factors in the range of 1–5 under small strains, associated with early percolation at sub-percent loadings, whereas graphene- or rGO-based photocurable composites often require higher filler concentrations and can reach gauge factors in the tens depending on network compactness and matrix rigidity. The GF ≈ 50 achieved for AESO/rGO falls within the upper range reported for rigid graphene-filled systems [67], while the moderate GF and superior cyclic stability observed for SPOT-E/CNT are characteristic of flexible CNT-based networks [19, 68]. Importantly, the present work extends beyond performance benchmarking by quantitatively correlating percolation behavior, nanoscale organization, segmental dynamics, and cyclic durability within a unified multiscale framework.

In summary, the two composites illustrate distinct sensing behaviors: SPOT-E/CNT composites provide moderate sensitivity with superior stability and mechanical compliance, whereas AESO/rGO composites deliver higher signal amplitude at the expense of structural robustness. These differences stem from the nanostructural organization discussed in the SANS section and the dispersion characteristics observed by SEM, with entangled CNT networks supporting more adaptable conductive pathways than the loosely stacked rGO aggregates. These contrasting behaviors also underscore the role of polymer matrix mechanical properties in determining piezoresistive response. SPOT-E, being softer and more ductile, accommodates strain without large network disruption, yielding low-to-moderate GF values ideal for stable and low-noise sensors. AESO, with its inherently higher stiffness, restricts deformation of the polymer chains and induces filler debonding under strain, amplifying resistance changes but reducing cycling stability. Literature reports similar performance for softer and rigid thermoplastic elastomers, where flexible matrices present lower mechanical hysteresis as well as lower GF, mainly for larger strains [69]. Consequently, the two systems address different application spaces: SPOT-E/CNT for robust and repeatable measurements in wearable or flexible electronics, and AESO/rGO for high-sensitivity detection in applications where small strain ranges and single-use sensing are required. Overall, this trade-off highlights the design space between sensitivity and durability in piezoresistive photocurable composites for sensor applications.

While individual trends observed in this work are consistent with previous reports on carbonaceous-filled photocurable systems, the conceptual advancement of the present study lies in the integration of multiscale experimental observations into a unified structure–processing–property framework. By directly correlating photopolymerization kinetics, nanoscale aggregation descriptors (SANS), polymer segmental dynamics (QENS), and macroscopic electrical and electromechanical behavior, this work demonstrates how curing inhibition and network heterogeneity propagate across length scales to govern functional performance. This integrated approach moves beyond validating isolated structure–property relationships and enables the identification of design-relevant trade-offs—such as sensitivity versus durability or curing efficiency versus percolation—that cannot be resolved using single-technique studies.

Overall, the quantitative descriptors extracted in this work further enable direct cross-scale correlations between processing, structure, and functional response. The lower percolation thresholds measured for CNT-based systems ($\varphi_c \approx 0.28$–0.30 wt.%) agree with their earlier viscosity increase and rapid formation of interconnected nanotube networks, while rGO composites require significantly higher loadings ($\varphi_c \approx 2.18$ wt.% and > 3 wt.% in AESO). This is consistent with larger aggregate dimensions and contact-dominated platelet stacking observed by SEM and SANS for rGO-based composites. The broader percolation transitions reflected by higher critical exponents (t up to ~ 5 for rGO systems) correlate with more heterogeneous network development and increased sensitivity to structural rearrangement under strain. In parallel, QENS results reveal increased segmental mobility in highly loaded AESO composites, what is in concordance with extended gelation times and the initial resistance drift observed during cyclic piezoresistive testing. Moreover, the lower mobility and sharper percolation behavior in SPOT-E/CNT systems are consistent with stable gauge factors (GF < 1) and minimal drift over around 700 cycles. These quantitative correlations reinforce the proposed multiscale structure–processing–property framework.

3 Conclusions

This work reports on the development of UV-curable nanocomposites reinforced with carbonaceous fillers by combining two photocurable matrices, SPOT-E (polyurethane acrylate flexible resin) and AESO (soybean oil-based rigid material), with carbon nanotubes (CNTs) and reduced graphene oxide (rGO) to investigate the interplay between matrix chemistry, filler dispersion, and multifunctional characteristics. CNTs inhibit photopolymerization above 0.6 wt%, whereas rGO allows complete curing up to 5 wt%, evidencing distinct filler–matrix interactions that govern curing and rheology. Structural analyses reveal better filler wetting and lower void density in SPOT-E, while AESO shows more compact aggregates and microvoids at high loadings, as confirmed by SEM and SANS, ultimately determining network formation and percolation behavior. Electrical conductivity increases by several orders of magnitude with filler content, reaching 0.014 S/m for SPOT-E/CNT and 7.4×10^{-5} S/m for AESO/rGO, while mechanical properties remain adequate for strain ranges relevant to sensing. Electromechanical measurements evidence distinct responses: SPOT-E/CNT composites exhibit stable, repeatable signals (GF < 1) suitable for durable, low-noise sensing, whereas AESO/rGO composites reach GF ≈ 50, offering high sensitivity for low-strain detection.

Overall, this work moves beyond a purely descriptive comparison of photocurable carbonaceous composites and establishes a multiscale structure–processing–property perspective by directly correlating photopolymerization behavior, nanoscale aggregate organization, polymer segmental dynamics, and macroscopic electromechanical performance. Importantly, CNT and rGO are not compared as equivalent fillers at identical concentrations, but are treated as distinct conductive network archetypes (1D CNT versus 2D rGO), and structure–property relationships are interpreted in terms of relative network development rather than absolute filler loading. By analyzing two matrices with fundamentally different mechanical nature and two representative filler network archetypes (1D CNT versus 2D rGO), the present study complements and extends previous reports on CNT- or graphene-filled UV-curable systems. Compared to earlier studies on individual CNT- or rGO-based UV-curable composites, the present work advances the field by providing a direct parallel analysis of 1D and 2D conductive network archetypes across matrices with distinct mechanical characteristics, integrating quantitative percolation analysis, nanoscale segmental dynamics (QENS), and cyclic electromechanical durability within a unified multiscale framework.

The results demonstrate that similar levels of electrical conductivity or piezoresistive sensitivity can originate from distinct network configurations, leading to different trade-offs between curing efficiency, mechanical integrity, sensitivity, and durability. These insights provide design-relevant guidance for tailoring photocurable composites toward specific functional requirements rather than relying on empirical filler optimization alone. In particular, the results indicate that elastic matrices combined with CNT-based conductive networks are preferable when long-term signal stability, mechanical compliance, and repeatability are required, such as in durable strain or deformation sensors. Conversely, rigid matrices combined with rGO networks are better suited for applications requiring high sensitivity at low strain levels, where limited durability and narrower operating windows can be tolerated. These explicit structure–processing–property relationships enable informed material selection and design depending on the targeted sensing performance and application constraints. Strategies such as improving filler dispersion through surface functionalization or compatibilizing agents, adjusting photoinitiator concentration to compensate for optical attenuation, and optimizing curing conditions to enhance crosslink uniformity could mitigate network heterogeneity and interfacial defects. Such approaches may enable higher conductive loadings while preserving mechanical integrity, representing a relevant direction for future development of UV-curable multifunctional composites.

Supplementary Information The online version contains supplementary material available at https://doi.org/10.1007/s42114-026-01770-2.

Acknowledgements The authors want also to thank the financial support from ISIS for the realization of experiment RB2410418 (https://doi.org/10.5286/ISIS.E.RB2410418). Technical and human support provided by SGIker (UPV/EHU, MICINN, GV/EJ, EGEF, and ESF) is gratefully acknowledged.

Author Contribution C. M. F. (Conceptualization, Data curation, Formal analysis, Funding acquisition, Investigation, Methodology, Validation, Writing – original draft), L. R. P. (Conceptualization, Data curation, Formal analysis, Methodology, Validation, Writing – review & editing), P. C. (Conceptualization, Data curation, Formal analysis, Funding acquisition, Investigation, Supervision, Writing – review & editing), V. P. (Data curation, Methodology, Validation, Writing –original draft, Writing – review & editing), L. P. C (Conceptualization, Data curation, Formal analysis, Validation, Writing – review & editing), M. Z. (Conceptualization, Data curation, Formal analysis, Methodology, Validation, Writing – review & editing), M. G. (Conceptualization, Data curation, Formal analysis, Investigation, Methodology, Validation, Writing – review & editing), J. P. (Conceptualization, Data curation, Funding acquisition, Supervision, Validation, Writing – review & editing), M. S. (Conceptualization, Funding acquisition, Project administration, Resources, Supervision, Writing – review & editing), S. L. M. (Conceptualization, Funding acquisition, Project administration, Resources, Supervision, Writing – review & editing).

Funding Open Access funding provided thanks to the CRUE-CSIC agreement with Springer Nature. C.M.F thanks financial support from the Basque Government Education (POS-E_2021_2_0001) and European Union's Horizon Europe research and innovation programmes under HORIZON-MSCA-2023-PF-01–01 PaSS (101153574). Financial support from the Basque Government under the ELKARTEK program is also acknowledged. This study forms part of the Advanced Materials program and was supported by MCIN with funding from European Union NextGenerationEU (PRTR-C17.I1) and by The Basque Government under the IKUR program. This work was supported by the Portuguese Foundation for Science and Technology (FCT) in the framework of the Strategic Funding UID/04650/2025 and contract 2023.07491. CEECIND (PC). M.G. and J.P. gratefully acknowledge financial support by the Estonian Research Council (grant: PRG 2772) and funding by the European Union under grant agreement No. 101159716.

Data Availability All data supporting the findings of this study are available within the paper and its Supplementary Information.

Declarations

Competing interests The authors declare no competing interests.

References

1. Bagheri A, Jin J (2019) Photopolymerization in 3D printing. ACS Appl Polym Mater. https://doi.org/10.1021/acsapm.8b00165
2. Yu K, Dunn ML, Qi HJ, Maute K (2025) Recent advances in design optimization and additive manufacturing of composites: from enhanced mechanical properties to innovative functionalities. NPJ Adv Manuf. https://doi.org/10.1038/s44334-025-00040-1
3. Peng X, Zhang J, Xiao P (2024) Photopolymerization approach to advanced polymer composites : integration of surface-modified nanofillers for enhanced properties. Adv Mater. https://doi.org/10.1002/adma.202400178
4. Mendes-felipe C, Oliveira J, Etxebarria I, Vilas-vilela JL (2019) State-of-the-art and future challenges of UV curable polymer-based smart materials for printing technologies. Adv Mater Technol. https://doi.org/10.1002/admt.201800618
5. Bauhofer W, Kovacs JZ (2009) A review and analysis of electrical percolation in carbon nanotube polymer composites. Compos Sci Technol 69:1486–1498. https://doi.org/10.1016/j.compscitech.2008.06.018
6. Potts JR, Dreyer DR, Bielawski CW, Ruoff RS (2011) Graphene-based polymer nanocomposites. Polymer 52:5–25. https://doi.org/10.1016/j.polymer.2010.11.042
7. Tilve-martinez D, Poulin P (2025) Vat photopolymerization 3D printing of conductive nanocomposites. Acc Mater Res. https://doi.org/10.1021/accountsmr.5c00060
8. Smith AD, Niklaus F, Paussa A, Der SS, Fischer AC, Sterner M, Wagner S, Vaziri S, Forsberg F, Esseni D, Mikael O, Lemme MC (2016). Piezoresistive Properties of Suspended. https://doi.org/10.1021/acsnano.6b02533
9. Uyguno T (2024) Piezoresistive and capacitive cement-based stress sensors designed by incorporating carbon nanotubes doped with graphene nanopowder for structural health monitoring. Sensors and Actuators : A Physical. https://doi.org/10.1016/j.sna.2024.115491
10. Mendes-felipe C, Oliveira J, Costa P, Ruiz-rubio L, Iregui A, González A (2019) Stimuli responsive UV cured polyurethane acrylated / carbon nanotube composites for piezoresistive sensing. Eur Polym J 120:109226. https://doi.org/10.1016/j.eurpolymj.2019.109226
11. Mendes-felipe C, Costa P, Roppolo I, Sangermano M (2022) Bio-Based Piezo- and Thermoresistive Photocurable Sensing Materials from Acrylated Epoxidized Soybean Oil 2100934:1–10. https://doi.org/10.1002/mame.202100934
12. Lima R, Serra J, Costa CM, Tubio CR, Nunes-pereira J, Lanceros-mendez S (2025) Effect of carbonaceous filler type and content on the piezoresistive response of screen-printed sustainable adhesive epoxy composites. React Funct Polym 215:106375. https://doi.org/10.1016/j.reactfunctpolym.2025.106375
13. Mukherjee A, Pulikkunnel PJ, Selenica S, Kamat AM, Birudula S, Kamperman M, Bose RK, Giri A, Kottapalli P (2026) Electrically conductive 3D-printed piezoresistive metastructure lattice sensors. ACS Appl Electron Mater. https://doi.org/10.1021/acsaelm.5c02422
14. Saadi OW, Khan KA (2025) Advancements in vat photopolymerization for piezoresistive sensors: materials, mechanisms, and applications. Virtual Phys Prototyp 20:1–37. https://doi.org/10.1080/17452759.2025.2505994
15. Martín-ayerdi A, Tropin T, Peřinka ˇN, Garamus VM, Soloviov D, Petrenko V, Lanceros-méndez S (2025) Synergetic effect of fullerene and fullerenol / carbon nanotubes in cellulose-based composites for electromechanical and thermoresistive applications. Polymers 17(24):3259. https://doi.org/10.3390/polym17243259
16. Mendes-felipe C, Cofano R, Garcia A, Sangermano M, Lanceros-mendez S (2023) Photocurable 3D printed anisotropic electrically

conductive materials based on bio-renewable composites. Addit Manuf 78:103867. https://doi.org/10.1016/j.addma.2023.103867
17. Lee T, Kim J, Siang C, Andreu A, Kim I, Lee W, Kim H, Su P, Yoon Y (2024) Prediction of curing depth dependence on CNT nanofiller dispersion for vat photopolymerization 3D printing. Chem Eng J 482:149110. https://doi.org/10.1016/j.cej.2024.149110
18. Idumah CI, Obele CM (2021) Understanding interfacial influence on properties of polymer nanocomposites. Surfaces and Interfaces 22:100879. https://doi.org/10.1016/j.surfin.2020.100879
19. Waqas O, Andreas S, Kumar SS (2023) Piezoresistive behavior of DLP 3D printed CNT / polymer nanocomposites under monotonic and cyclic loading. Int J Adv Manuf Technol. https://doi.org/10.1007/s00170-023-11123-8
20. Arias-ferreiro G, Ares-pernas A, Lasagabáster-latorre A, Dopico-garcía MS, Ligero P, Pereira N, Costa P, Abad M (2022) Photocurable printed piezocapacitive pressure sensor based on an acrylic resin modified with polyaniline and lignin. Adv Mater Technol. https://doi.org/10.1002/admt.202101503
21. Cho J, Lee H, Nam K, Yeo H, Yang C, Gi D, Lee D, Yun S (2020) Enhanced electrical conductivity of polymer nanocomposite based on edge-selectively functionalized graphene nanoplatelets. Compos Sci Technol 189:108001. https://doi.org/10.1016/j.compscitech.2020.108001
22. Cosola A, Sangermano M, Terenziani D, Conti R, Messori M, Grützmacher H, Fabrizio C, Chiappone A (2021) DLP 3D – printing of shape memory polymers stabilized by thermoreversible hydrogen bonding interactions. Appl Mater Today 23:101060. https://doi.org/10.1016/j.apmt.2021.101060
23. Porcarello M, Mendes-felipe C, Lanceros-mendez S, Sangermano M (2024) Design of acrylated epoxidized soybean oil biobased photo-curable formulations for 3D printing. Sustain Mater Technol 40:e00927. https://doi.org/10.1016/j.susmat.2024.e00927
24. Zeinabad HA, Zarrabian A, Saboury AA, Alizadeh AM (2016) Interaction of single and multi wall carbon nanotubes with the biological systems : tau protein and PC12 cells as targets. Nat Publ Gr. https://doi.org/10.1038/srep26508
25. YaqoobS, Ali Z, Ali S, Amore AD (2025) Polystyrene – carbon nanotube composites : interaction mechanisms, preparation methods, structure, and rheological properties — a review. Physchem 5(2):14. https://doi.org/10.3390/physchem5020014
26. Reynolds J, Unterhalter J, Francoeur M, Bortner M, Raeymaekers B (2024) Viscosity of mono- and polydisperse mixtures of photopolymer and rigid spheres for manufacturing of engineered composite materials using vat photopolymerization. Adv Eng Mater. https://doi.org/10.1002/adem.202301630
27. Shi H, Zhuang Q, Zheng A, Guan Y, Wei D, Xu X (2023) Study of the radical polymerization mechanism and its application in the preparation of highperformance PMMA by reactive extrusion. RSC Adv 13:7225–7236. https://doi.org/10.1039/d2ra06441c
28. Bodor M, Lasagab A, Arias-ferreiro G (2024) Improving the 3D printability and mechanical performance of biorenewable soybean oil-based photocurable resins. Polymers 16(7):977. https://doi.org/10.3390/polym16070977
29. Majidian M, Magrez A, Forró L, Leterrier Y (2021) Viscoelastic behavior of suspensions of reduced graphene oxide nanoparticles in epoxy. Appl Phys Lett 119:041901. https://doi.org/10.1063/5.0059951
30. Martina S, Sevriugina V, Pavlin D, Lepcio P (2023) Matching low viscosity with enhanced conductivity in vat photopolymerization 3D printing : disparity in the electric and rheological percolation thresholds of carbon-based nanofillers is controlled by the matrix type and filler dispersion. ACS Omega. https://doi.org/10.1021/acsomega.3c05683
31. Gharghouri MA (2016) Chapter 8. Incoherent neutron scattering. Neutron scattering and other nuclear techniques for hydrogen in materials. Springer International Publishing, Switzerland, pp 227–244. https://doi.org/10.1007/978-3-319-22792-4_8
32. Bailey EJ, Gri PJ, Tyagi M, Winey KI (2019) Segmental diffusion in attractive polymer nanocomposites: a quasi-elastic neutron scattering study. Macromolecules 52:669–678. https://doi.org/10.1021/acs.macromol.8b01716
33. Kruteva M, Genix A, Holderer O, Oberdisse J (2022) Recent scattering approaches to structure and dynamics of polymer nanocomposites. Frontiers in Soft Matter. https://doi.org/10.3389/frsfm.2022.992563
34. Golub M, Pieper J, Telling MTF, Seydel T, Frick B, Benetti AR, Bordallo HN (2025) Dynamics of hydrogen-rich species in light-cured dental materials. Polymer 339:129134. https://doi.org/10.1016/j.polymer.2025.129134
35. Andrijanto E, Shoelarta S, Subiyanto G, Rifki S (2016) Facile Synthesis of Graphene from Graphite Using ascorbic acid as reducing agent. AIP Conf Proc 1725:020003. https://doi.org/10.1063/1.4945457
36. Larissa T, Cristóvan FH, Lemes AP. (2015) Effect of MWCNT functionalization on thermal and electrical properties of PHBV / MWCNT nanocomposites. 55–65. https://doi.org/10.1557/jmr.2014.303.
37. Mendes-felipe C, Garcia A, Salazar D, Vilas-vilela JL, Lanceros-mendez S (2021) Composites part C : open access photocurable magnetic materials with tailored functional properties. Compos Part C Open Access 5:100143. https://doi.org/10.1016/j.jcomc.2021.100143
38. Cardoso P, Silva J, Klosterman D, Covas JA, Van Hattum FWJ, Simoes R, Lanceros-mendez S (2012) The role of disorder on the AC and DC electrical conductivity of vapour grown carbon nanofibre / epoxy composites. Compos Sci Technol 72:243–247. https://doi.org/10.1016/j.compscitech.2011.11.008
39. Milner EM, Skipper NT, Howard CA, Sha MSP, Buckley DJ, Rahnejat KA, Cullen PL, Heenan RK, Lindner P, Schweins R (2012) Structure and morphology of charged graphene platelets in solution by small-angle neutron scattering. J Am Chem Soc. https://doi.org/10.1021/ja211869u
40. Mendes-felipe C, Carvalho R, Martins P, Ivankov OI, Bobrikov I, Petrenko V, Porro JM, Sangermano M, Lanceros-mendez S (2023) Photocurable hybrid materials with high magnetodielectric coupling. ACS Appl Polym Mater. https://doi.org/10.1021/acsapm.3c01566
41. Schmidt BYPW (1991) Small-angle scattering studies of disordered, porous and fraetal systems. J Appl Cryst 24(5):414–435. https://doi.org/10.1107/S0021889891003400
42. Kenderesi V, Achour ME, Boukheir S, Costa LC, Oueriagli A, Outzourhit A (2017) Structural characterization and electrical properties of carbon nanotubes / epoxy polymer composites 44514:1–8. https://doi.org/10.1002/app.44514
43. Izgorodina EI, Tabor RF (2018) Bulk properties of aqueous graphene oxide and reduced graphene oxide with surfactants and polymers : adsorption and stability †. Phys Chem Chem Phys. https://doi.org/10.1039/c8cp02738b
44. Tiihonen LV, Weir MP, Parnell AJ, Boothroyd SC, Johnson DW, Dalgliesh RM, Bleuel M, Duif CP, Bouwman WG, Thompson RL, Coleman KS, Clarke N, Hamilton WA, Washington AL, Parnell SR (2024) Revealing microscale bulk structures in polymer – carbon nanocomposites using spin-echo SANS. Soft Matter. https://doi.org/10.1039/d4sm00578c
45. Govindaraj P, Sokolova A, Salim N, Juodkazis S, Konstantin F, Fox B, Hameed N (2021) Distribution states of graphene in polymer nanocomposites : a review. Compos Part B Eng 226:109353. https://doi.org/10.1016/j.compositesb.2021.109353
46. Tarfaoui M, Lafdi K, El Moumen A (2016) Mechanical properties of carbon nanotubes based polymer composites. Compos Part B Eng 103:113–121. https://doi.org/10.1016/j.compositesb.2016.08.016

47. Sokhandani N, Bavi O, Zebarjad S, Setoodeh A (2025) Results in engineering experimental investigation and semi-empirical modeling of mechanical behavior in Gr, GO, and rGO nanocomposites. Results Eng 26:105290. https://doi.org/10.1016/j.rineng.2025.105290
48. Yan N, Buonocore G, Lavorgna M, Kaciulis S, Kiran S, Zhan Y, Xia H, Ambrosio L (2014) The role of reduced graphene oxide on chemical, mechanical and barrier properties of natural rubber composites. Compos Sci Technol 102:74–81. https://doi.org/10.1016/j.compscitech.2014.07.021
49. Georgousis G, Pandis C, Kalamiotis A, Georgiopoulos P, Kyritsis A, Kontou E, Pissis P (2015) Strain sensing in polymer / carbon nanotube composites by electrical resistance measurement. Compos Part B 68:162–169. https://doi.org/10.1016/j.compositesb.2014.08.027
50. Oseli A, Tomkovi T, Hatzikiriakos SG, Vesel A, Arzen M (2023) Carbon nanotube network formation and configuration / morphology on reinforcing and conductive performance of polymer-based nanocomposites. Compos Sci Technol. https://doi.org/10.1016/j.compscitech.2023.110010
51. Daniel D, Lee J, Park J, Choi W (2022) High-resolution and electrically conductive three-dimensional printing of carbon nanotube-based polymer composites enabled by solution intercalation. Carbon 194:1–9. https://doi.org/10.1016/j.carbon.2022.03.042
52. Wu Q, Sundborg H, Andersson RL, Peuvot K, Nilsson F, Hedenqvist MS, Olsson RT (2017) Conductive biofoams of wheat gluten containing carbon nanotubes, carbon black or reduced graphene oxide. RSC Adv. https://doi.org/10.1039/c7ra01082f
53. Capezza A, Andersson RL, Stro V, Wu Q, Sacchi B, Farris S, Hedenqvist MS, Olsson RT (2019) Preparation and comparison of reduced graphene oxide and carbon nanotubes as fillers in conductive natural rubber for flexible electronics. ACS Omega. https://doi.org/10.1021/acsomega.8b03630
54. Tang Z, Wang D, Li Y, Huang P, Fu S (2022) Modeling the synergistic electrical percolation effect of carbon nanotube / graphene / polymer composites. Compos Sci Technol 225:109496. https://doi.org/10.1016/j.compscitech.2022.109496
55. Dios JR, García-Astrain C, Costa P, Viana JC, Lanceros-Méndez S (2019) Carbonaceous filler type and content dependence of the physical-chemical and electromechanical properties of thermoplastic elastomer polymer composites. Materials 12:1405
56. Li J, Kim J (2007) Percolation threshold of conducting polymer composites containing 3D randomly distributed graphite nanoplatelets. Compos Sci Technol 67:2114–2120. https://doi.org/10.1016/j.compscitech.2006.11.010
57. Costa P, Nunes-pereira J, Oliveira J, Silva J, Moreira JA, Carabineiro SAC, Buijnsters JG, Lanceros-mendez S (2017) High-performance graphene-based carbon nano fi ller / polymer composites for piezoresistive sensor applications. Compos Sci Technol 153:241–252. https://doi.org/10.1016/j.compscitech.2017.11.001
58. Seesaard T, Wongchoosuk C (2021) Flexible and stretchable strain and pressure sensors: from basic principles to state-of-the-art applications. Micromachines 14(8):1638. https://doi.org/10.3390/mi14081638
59. Haghgoo M, Ansari R, Hassanzadeh-aghdam MK (2022) Prediction of piezoresistive sensitivity and percolation probability of synergetic CNT-GNP conductive network composite. Sens Actuators A Phys 336:113414. https://doi.org/10.1016/j.sna.2022.113414
60. Cohen DJ, Mitra D, Peterson K, Maharbiz MM (1825) A Highly Elastic, Capacitive Strain Gauge Based on Percolating Nanotube. Networks 2012:8–12
61. Xu S, Fan Z, Li C, Wang P, Abdul K, Pan L (2019) Investigation of strain sensing mechanisms on ultra-thin carbon nanotube networks with different densities. Carbon 155:421–431. https://doi.org/10.1016/j.carbon.2019.09.004
62. Costa P, Gonc S, Mora H, Carabineiro SAC, Viana JC (2019) Highly sensitive piezoresistive graphene-based stretchable composites for sensing applications. ACS Appl Mater Interfaces. https://doi.org/10.1021/acsami.9b19294
63. Krieg AS, King JA, Jaszczak DC, Miskoglu I, Mills OP, Odegard GM (2018) Tensile and conductivity properties of epoxy composites containing carbon black and graphene nanoplatelets. J Compos Mater. https://doi.org/10.1177/0021998318771460
64. WuZ, Wei J, Dong R, Chen H (2019) Epoxy composites with reduced graphene oxide – cellulose nanofiber hybrid filler and their application in concrete strain and crack monitoring. Sensors 19(18):3963. https://doi.org/10.3390/s19183963
65. Chen C, Guo J (2026) Lcd 3D printing of conductive photo-nanocomposite for a piezoresistive component integrated with wearable rings. Sens Actuators A Phys 401:117586. https://doi.org/10.1016/j.sna.2026.117586
66. Olivieri F, Rollo G, De Falco F, Avolio R, Bonadies I, Castaldo R, Cocca M, Emanuela M, Marino E, Gennaro L (2023) Reduced graphene oxide/polyurethane coatings for wash-durable wearable piezoresistive sensors. Cellulose 30:2667–2686. https://doi.org/10.1007/s10570-023-05042-w
67. Ca E, Garcia JR, Suilleabhain DO, Gabbett C, Carey T, Coleman JN (2022) Quantifying the piezoresistive mechanism in high-performance printed graphene strain sensors. ACS Appl Mater Interfaces 14:7141–7151. https://doi.org/10.1021/acsami.1c21623
68. Cortes A, Sanchez-Romate XF, Jimenez-Suarez A, Campo M, Ureña A, Prolongo SG (2020) Mechanical and strain-sensing capabilities of carbon nanotube reinforced composites by digital light processing 3D printing technology. Polymers (Basel) 12:975
69. Costa P, Ribeiro S (2015) Mechanical vs. electrical hysteresis of carbon nanotube / styrene – butadiene – styrene composites and their influence in the electromechanical response. Compos Sci Technol 109:1–5. https://doi.org/10.1016/j.compscitech.2015.01.006